Geophysical Journal International

Geophys. J. Int. (2013) **195,** 1384–1394
Advance Access publication 2013 September 3

doi: 10.1093/gji/ggt318

Crustal attenuation characteristics in western Turkey

Tevfik Özgür Kurtulmuş[1,2] and Nihal Akyol[1]

[1] *Dokuz Eylül University, Faculty of Engineering, Department of Geophysical Engineering, Tınaztepe Campus, TR* 35397 *Buca-Izmir, Turkey*
[2] *Dokuz Eylül University, the Graduate School of Natural and Applied Sciences, Department of Geophysical Engineering, Tınaztepe Campus, TR* 35397 *Buca-Izmir, Turkey. E-mail: ozgur.kurtulmus@deu.edu.tr*

Accepted 2013 August 6. Received 2013 August 2; in original form 2013 May 9

SUMMARY

We analysed 1764 records produced by 322 micro- and moderate-size local earthquakes in western Turkey to estimate crustal attenuation characteristics in the frequency range of $1.0 \leq f \leq 10$ Hz. In the first step, we obtained non-parametric attenuation functions and they show that seismic recordings of transverse and radial *S* waves exhibit different characteristics at short and long hypocentral distances. Applying a two-step inversion, we parametrized $Q(f)$ and geometrical spreading exponent $b(f)$ for the entire distance range between 10 and 200 km and then we estimated separately Q and b values for short (10–70 km) and large (120–200 km) distance ranges. We could not observe significant frequency dependencies of b for short distance range, whereas the significant frequency dependence of b was observed for large distances. Low Q_0 values (∼60) with strong frequency dependence of Q (∼1.4) for short distances suggest that scattering might be an important factor contributing to the attenuation of body waves in the region, which could be associated to a high degree of fracturing, fluid filled cracks, young volcanism and geothermal activity in the crust. Weak Q frequency dependence and higher Q_0 values for large distances manifest more homogenous medium because of increasing pressure and enhanced healing of cracks with increasing temperature and depth. Q anisotropy was also observed for large hypocentral distance ranges.

Key words: Elasticity and anelasticity; Seismic anisotropy; Seismic attenuation; Europe.

GJI Seismology

1 INTRODUCTION

The central part of west Turkey has experienced extensional tectonics since Late Oligocene times and the region includes a well-developed metamorphic core complex, the Menderes Massif (e.g. Gessner *et al.* 2001; Seyitoğlu & Işık 2009). The Massif is one of the Alpine metamorphic belts, where high-grade metamorphic rocks of the middle to lower crust are now exposed at the surface. Post-collisional extension in the region caused it to be exhumed. The Menderes Massif consists of pre-Cambrian and Palaeozoic to Lower Tertiary metamorphic rocks (e.g. Şengör *et al.* 1984; Rojay *et al.* 2005). During the Early-Middle Miocene period thick volcanosedimentary associations were formed within approximately *NS*-trending fault-bounded continental basins under an *E–W* extensional regime (Yılmaz *et al.* 2000). The Late Miocene volcanism was marked by alkali basalts and basanites erupted along the zones of localized extension in the region (Aldanmaz 2002). The current extension in ∼*N–S* direction proceeds at a rate of 30–40 mm yr^{-1} (Oral *et al.* 1995). The Gediz, Küçük Menderes and Büyük Menderes grabens, separated by the Bozdağ and Aydın Mountain Horsts, are the most prominent neotectonic structures of the region (Figs 1 and 2). Each graben is a composite basin and comprises several subbasins with sediment thicknesses being more than 3000 m in some locations (Çiftçi *et al.* 2010).

One of the fundamental requirements for seismic-hazard assessment is accurate knowledge of attenuation effects (Sonley & Atkinson 2006), which lead us to carry out this study for western Turkey. Together with high seismicity related to active extensional tectonics and densely populated areas on deep basin/graben structures, seismic hazard studies have become progressively more important for the earthquake engineering applications in the region. Up to now, seismic attenuation properties of western Turkey have been studied utilizing different kinds of waves and methods. For instance Akıncı *et al.* (1994) measured the attenuation of coda waves in western Turkey as a function of lapse time for a broad set of lapse times (30–190 s). They observed that the average coda quality factor Q_c depends strongly on lapse time and frequency. Several other researchers investigated the attenuation mechanism in western/northwestern Turkey (e.g. Akıncı *et al.* 1995a,b, 2004; Akyol *et al.* 2002; Bindi *et al.* 2006), southwestern Turkey (e.g. Şahin *et al.* 2007, 2013; Şahin 2008) and the Marmara region (e.g. Horasan *et al.* 1998; Kaşlılar-Özcan *et al.* 2002; Horasan & Boztepe-Güney 2004).

This paper presents empirical attenuation functions that characterize the amplitude decay for the central part of west Turkey. We made independent estimates of the attenuation using the transversely polarized (*SH*) and vertically polarized (*SV*) *S* waves. The attenuation functions, including anelasticity of heterogeneous media and geometrical spreading effects, were obtained using a non-parametric

© The Authors 2013. Published by Oxford University Press on behalf of The Royal Astronomical Society.

Downloaded from https://academic.oup.com/gji/article/195/2/1384/653885 by Dokuz Eylul University Library (DEU) user on 02 September 2021

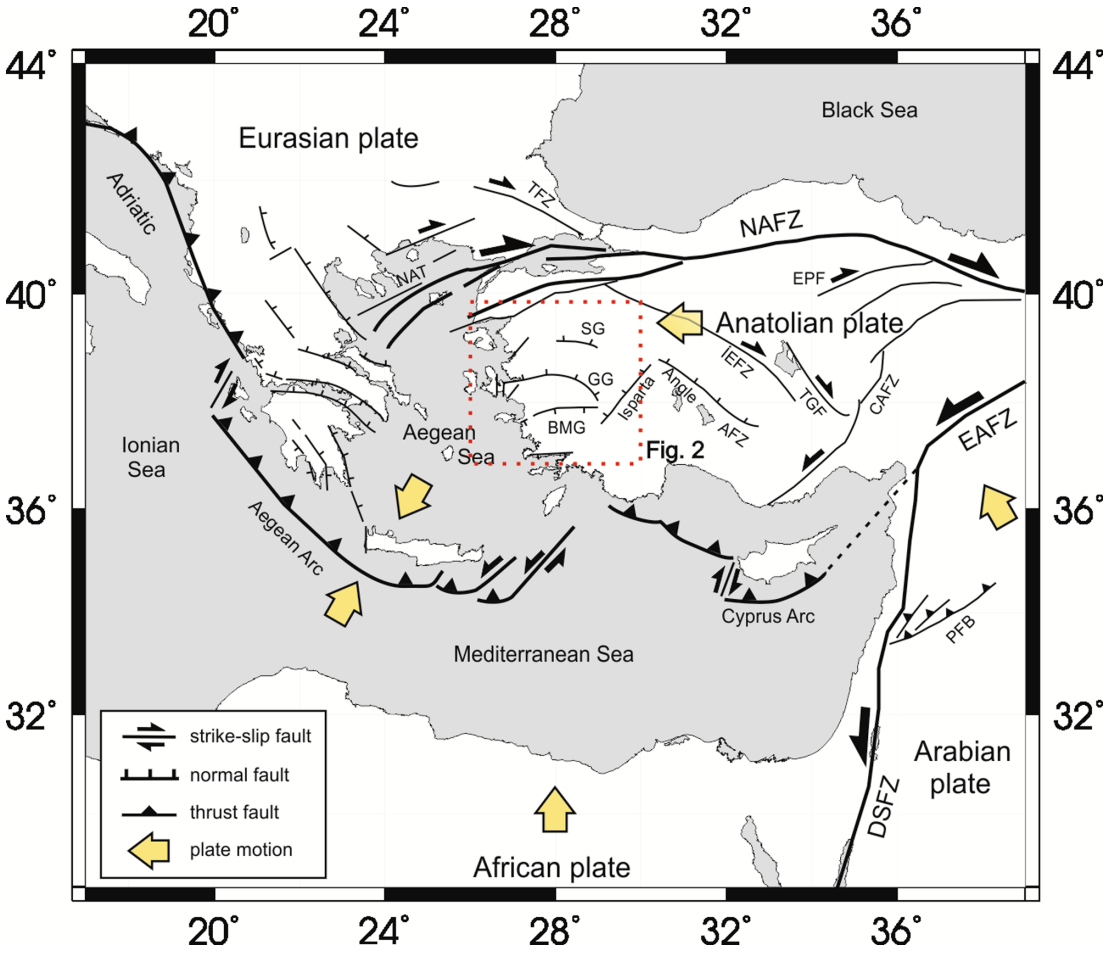


Figure 1. The major neotectonic structures and plate tectonics of western Turkey. DSFZ, Dead Sea Fault Zone; PFB, Palmyride Fold Bend; EAFZ, East Anatolian Fault Zone; NAFZ, North Anatolian Fault Zone; CAFZ, Central Anatolian Fault Zone; EPF, Ezinepazarı Fault; TGF, Tuzgölü Fault; İEFZ, İnönü-Eskişehir Fault Zone; AFZ, Akşehir Fault Zone; BMG, Büyük Menderes Graben; GG, Gediz Graben; SG, Simav Graben; NAT, North Anatolian Through; TFZ, Thrace Fault Zone. Large arrows indicate relative plate motion directions with respect to Eurasia (after Uzel *et al.* 2012). The area with red dashed lines shows the region of Fig. 2.

approach described by Castro *et al.* (1990). These functions were then used to parametrize Q and the geometrical spreading exponent b with a two-step inversion. We performed all calculations for three different distance ranges (10–200 km, 10–70 km and 120–200 km) to separate deeper and longer ray path effects from shallow and near ones. The main goal of these analyses is to evaluate the crustal attenuation characteristics with regard to frequency dependence of both Q and b values for the region.

2 DATA

We used the Western Anatolia Seismic Recording Experiment (WASRE; Akyol *et al.* 2006; Zhu *et al.* 2006a,b) network data, recorded with 5 STS-2 broadband and 24 Mark L-22 short-period (2 Hz), three-component sensors in between November 2002 and October 2003. Two different array configurations were used during this experiment. The details about array configuration and also instrumentation were given beforehand by Akyol *et al.* (2006, 2013) and Zhu *et al.* (2006a). Fig. 2 shows the locations of the stations and earthquakes used in this study. Our data set includes events with local magnitudes ranging from 2.0 to 5.6, hypocentral distances range between 3.5 and 205 km and focal depths range from 1.4 to 27 km (Fig. 3). The station list including geological units on which they were deployed and initial data processing stages were given by Akyol *et al.* (2013). Site effects obtained by two different spectral ratio methods were also given by Akyol *et al.* (2013). *S*-wave amplitudes used in the inversion were restricted to stations having at least ten records and to earthquakes recorded by at least three stations. We evaluated 1764 three-component recordings for 322 events. The time window starting with *S*-wave arrival was selected as 7 s and Fourier transform was computed after applying a 5 per cent cosine tapered window. The spectra were smoothed with a 9-point moving average operator and then a non-parametric inversion scheme (Castro *et al.* 1990) was applied to the data.

3 METHOD AND RESULTS

We characterized the spectral amplitude decay versus hypocentral distance using a non-parametric model (Castro *et al.* 1990):

$$D_i(f,r) = M_i(f)A(f,r), \quad (1)$$

where $D_i(f,r)$ represents the observed spectral amplitude for event i, whereas $A(f,r)$ and $M_i(f)$ represent the attenuation function and source term, respectively. $M_i(f)$ is a scalar (one for each earthquake i at frequency f) that depends on the size of the earthquake. In this approach, $A(f,r)$ is constrained to be a smooth function of

Downloaded from https://academic.oup.com/gji/article/195/2/1384/653885 by Dokuz Eylul University Library (DEU) user on 02 September 2021

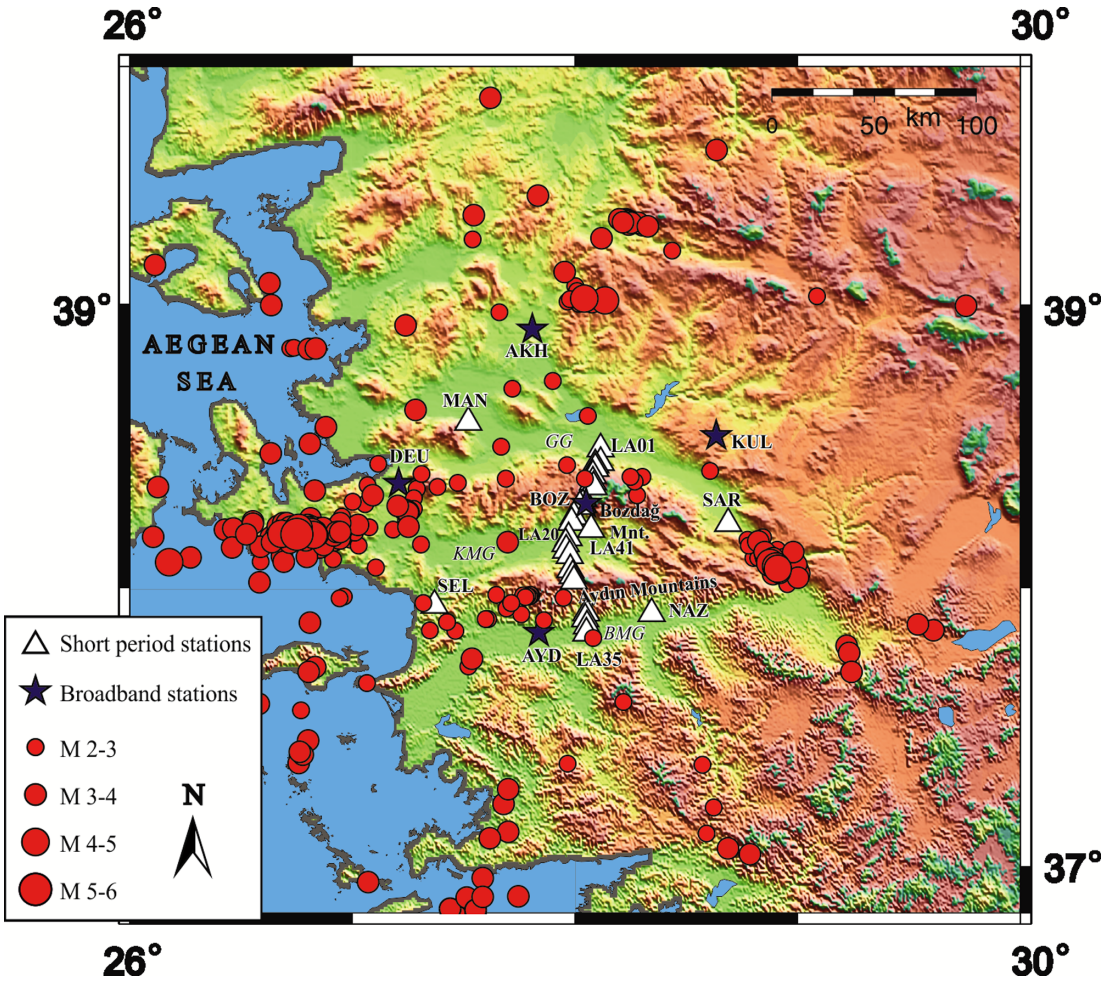


Figure 2. Locations of the stations and distribution of earthquakes (red dots) used in this study. White triangles and blue stars indicate short period and broad-band stations of WASRE network, respectively. GG, Gediz Graben; KMG, Küçük Menderes Graben; BMG, Büyük Menderes Graben.

hypocentral distance, with a value of 1 at $r = 0$. This equation can be linearized as:

$$\log D_{ij}(f, r) = \log m_i(f) + \log A_j(f, r), \tag{2}$$

By using the eq. (2), we calculated non-parametric attenuation functions including geometrical spreading and Q effects for 12 frequencies between 1.0 and 10 Hz. We performed all calculations for *SH* and *SV* waves using singular value decomposition (SVD) method (Menke 1989).

Fig. 4 shows observed spectral amplitudes for an $M_L = 4.3$ event along with estimated amplitude decrease for the transverse *S* wave. The attenuation functions were obtained by simultaneously inverting all data from 322 events. The dispersion of the data could be attributed to site response of the stations used (Castro *et al.* 1999). Fig. 5 shows the estimated non-parametric attenuation functions for *SH* and *SV* waves. Apparent lack of attenuation was observed between 70 and 120 km. The slopes of attenuation curves show significant changes for 10–70 and 120–200 km distance ranges at lower frequencies. rms values of the residuals associated with the inversion results are given in Fig. 6.

3.1 Parametrization of attenuation functions *A(f,r)*

To separate Q and geometrical spreading exponent b, we applied a two-step inversion to the non-parametric attenuation functions. The total attenuation could be parametrized as a product of two functions representing different attenuation mechanisms (Castro *et al.* 1990, 1999, 2008a):

$$A(f, r) = G(r)e^{-\pi fr/vQ}, \tag{3}$$

where *A(f,r)* represents the attenuation curve at a fixed frequency *f*. The first right-hand term accounts for geometrical spreading;

$$G(r) = \frac{1}{r^b}. \tag{4}$$

The theory predicts that $G(r) = 1/r$ and $b = 1$ for body waves. However, the geometrical spreading of regional phases is a complicated function of crustal and upper mantle velocity structure (Sereno & Given 1990). Many studies of body-wave attenuation (e.g. Ibáñez *et al.* 1993; Castro *et al.* 2008b, 2009) show that the geometrical spreading coefficient associated with distance may be more complicated than a simple assumption of $b = 1$; this is because of the complex velocity structure of the medium (e.g. Olafsson *et al.* 1998; Akıncı *et al.* 2006; Padhy 2009). The geometrical spreading models are path specific and depend on several factors, such as focal depth, crustal thickness, crustal velocity gradient and the existence of a strong discontinuity, etc. (Akıncı *et al.* 2006).

The second right-hand term of eq. (3) is for amplitude decrease because of total Q (intrinsic and scattering). To describe the

Downloaded from https://academic.oup.com/gji/article/195/2/1384/653885 by Dokuz Eylul University Library (DEU) user on 02 September 2021

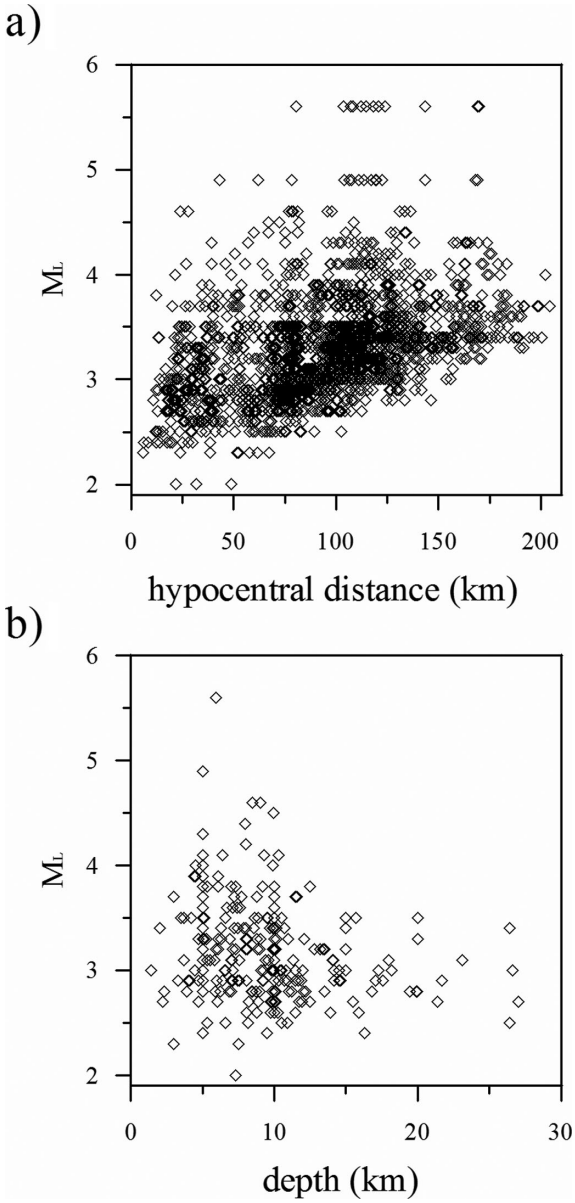


Figure 3. The distributions of local magnitudes versus (a) hypocentral distances and (b) depths of earthquakes.

observed frequency dependence of the estimated values of Q, we used the functional form:

$$Q(f) = Q_0 f^n, \tag{5}$$

where Q_o is the value of Q at 1 Hz and n is the Q frequency dependence. The parameter v in eq. (3) is the average S-wave velocity, based on the crustal structure, given by Akyol *et al.* (2006) for the region. Eq. (3) can be written as:

$$\log A(f, r) = -b \log(r) - \frac{\pi f}{vQ} r \log(e). \tag{6}$$

Assuming that residuals in eq. (1) is the product of source spectra and site response and near-surface propagation effects are carried by the site term, and also the source term probably includes the array coverage of the near-surface attenuation effect (e.g. Castro *et al.* 1990, 1999, 2008a), we modelled the attenuation functions as the form in eq. (3). Some researchers have been modelled an array average of near-surface attenuation values (e.g. Malagnini *et al.* 2002; Akıncı *et al.* 2006) as in the excitation terms which depends on source characteristic such as the energy released and is valid for the average site class. On the other hand, some others have been modelled frequency dependence of near-surface attenuation (e.g. Castro *et al.* 2008b,c, 2009) as being the third right-hand term in eq. (3).

Because there is not enough data at the distance smaller than 10 km (see Fig. 3), $A(f,r)$ functions were normalized at 10 km for each fixed frequency. Fig. 7 shows obtained Q and b values of the *SH* and *SV* waves for the entire distance range. The frequency-dependent values for Q are $Q_{SH}(f) = 177.29(\pm 12.34) f^{0.65(\pm 0.04)}$ and $Q_{SV}(f) = 200.32(\pm 18.21) f^{0.63(\pm 0.06)}$. Slight decrease in b for the *SH* and *SV* waves was observed at the frequencies higher than 2 Hz. Because of an apparent lack of attenuation between 70 and 120 km, we decided to separately perform Q and b estimates for short (10–70 km) and large (120–200 km) distance ranges. Fig. 8 shows Q estimates for the *SH* and *SV* waves for short and large distances. The frequency dependencies of Q are $Q_{SH}(f) = 60.97(\pm 7.92) f^{1.42(\pm 0.08)}$ and $Q_{SV}(f) = 57.55(\pm 6.51) f^{1.46(\pm 0.07)}$ for short distances, and $Q_{SH}(f) = 113.45(\pm 7.81) f^{0.47(\pm 0.04)}$ and $Q_{SV}(f) = 173.60(\pm 11.29) f^{0.28(\pm 0.04)}$ for large distances.

The frequency dependencies of b for two different distance ranges are given in Fig. 9. The arithmetic mean values of the *SH* and *SV* waves b estimates are 0.88 ± 0.03 for short distances. The b estimates beyond 2 Hz have significant decrease with increasing frequency for long distances (Fig. 9b). Note that *rms* values of residuals associated with the second inversion step in eq. (6) are given in Fig. 10. As shown in this figure, *rms* values of residuals for short and large distances are smaller than entire distance ones at the frequencies larger than 4.0 Hz.

4 DISCUSSION

The general characteristics of the empirical attenuation functions that we obtained for the entire distance range are shown in Figs 4 and 5. The slope of the decay is significant for short (10–70 km) and large (120–200 km) distance ranges. An apparent lack of attenuation between 70 and 120 km might be originated from the lower crustal/Moho reflections such as the contribution of the *SmS* phases (e.g. Atkinson & Mereu 1992; Akıncı *et al.* 2006). Boztepe-Güney & Horasan (2002) and Bindi *et al.* (2006) interpreted similar observations as a characteristic feature of crustal propagation in northwestern Turkey caused by critical Moho reflections, although the hinge points of obtained curves are unique to the crustal attenuation and velocity structure of the region of interest. According to Yang *et al.* (2007), the character of attenuation functions typically changes where the near-critical Moho reflections disrupt the uniform-space approximations. Fig. 5 compares the non-parametric attenuation functions of the *SH* and *SV* waves. The slight differences in the amount of attenuation between transverse and radial components, especially for high frequencies, might be associated to near-surface fluid saturated sediments or cracks. On the other hand, these small differences are within the statistical uncertainties of the estimates (Fig. 6).

We estimated Q and b values for the entire distance range of interest. As can be seen in Fig. 7, anelastic attenuation and geometrical spreading exponent are very close for the *SH* and *SV* waves. An average Q of them is $Q(f) = 189.63(\pm 13.50) f^{0.64(\pm 0.05)}$. High frequency dependence of Q values has been reported for tectonically active regions in Turkey (e.g. Akıncı *et al.* 1994; Akıncı & Eyidoğan 1996; Cong & Mitchell 1998; Horasan *et al.* 1998;

Downloaded from https://academic.oup.com/gji/article/195/2/1384/653885 by Dokuz Eylul University Library (DEU) user on 02 September 2021

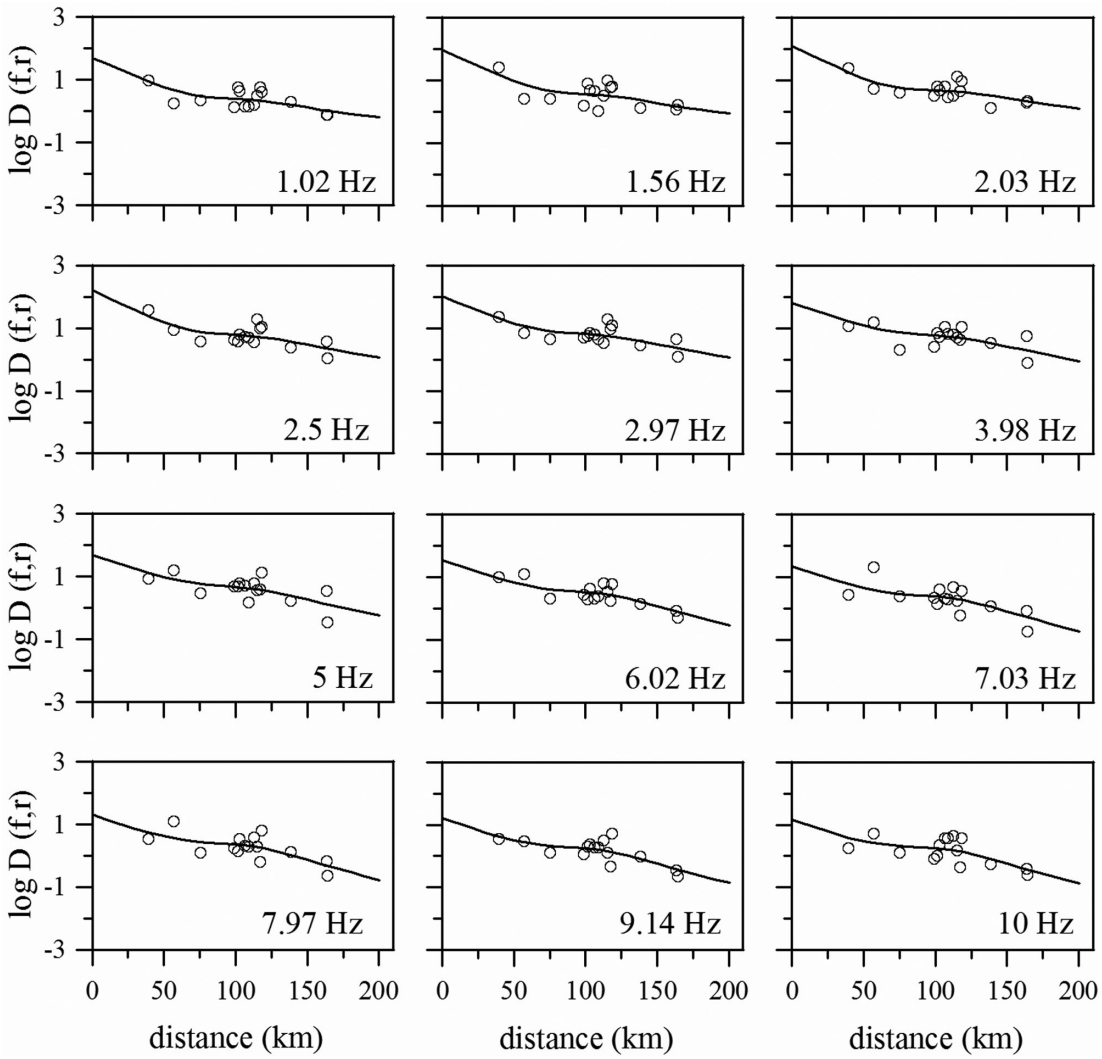


Figure 4. Observed spectral amplitudes (circles) for an event ($M_L = 4.3$) and estimated amplitude decrease of *SH* waves (solid lines) for each fixed frequency.

Horasan & Boztepe-Güney 2004). Low Q_o values could be related to possible mid-crustal low-velocity layer previously mentioned for the region (Saunders *et al.* 1998; Akyol *et al.* 2006; Gürer & Bayrak 2007). Zor *et al.* (2007) obtained low L_g Q_o values for the eastern Anatolian Plateau (∼70–100) and for the Menderes Massif (∼60–150) in western Turkey. For the eastern Anatolian Plateau, they related these results with localized mid-crustal low-velocity zones (Zor *et al.* 2003), which might be an indication of partial melt in the crust. Similarly, low L_g Q_o values along the Menderes massif were associated with the partially molten crust and young volcanism by Şahin *et al.* (2013).

The exponent b changes from 1.0 to 0.7 with increasing frequency for the entire distance range (Fig. 7). However, F-test statistics reveal that there are no statistically meaningful linear trends between the exponent b values in the frequency range of interest. For that reason, we parametrize $b(f)$ values for two different frequency ranges: an average value of $b = 0.97$ (± 0.02) for $f \leq 2$ Hz; $b(f) = 1.10(\pm 0.03)$ $f^{-0.19(\pm 0.02)}$ for $f > 2$ Hz for *SH* waves and an average value of $b = 0.99$ (± 0.01) for $f \leq 2$ Hz; $b(f) = 1.10(\pm 0.03)$ $f^{-0.18(\pm 0.01)}$ for $f > 2$ Hz for *SV* waves. Slight decrease in b beyond 2 Hz could be attributed to constructive interference of high-frequency waves. These parametrizations could be adequate for the region within the frequency range of 1–10 Hz.

Fig. 8 shows Q estimates for short and large distances. The Q-frequency dependence for large distance range is lower than the one obtained for short distances. These results indicate that *S* phases recorded at long distance range propagate through more homogenous deeper media. Controversially, stronger frequency dependence of Q at short distance range underlines the heterogeneity which could be associated to high degree of fracturing (e.g. Akyol *et al.* 2006; Çiftçi *et al.* 2010), extensive volcanism (e.g. Tokçaer *et al.* 2005; Aldanmaz 2006) and fluid filled cracks/geothermal systems (e.g. Tarcan *et al.* 2000; Mutlu 2007) in the crust. Akıncı *et al.* (1995b) separated the effects of intrinsic and scattering attenuation in western Turkey using a Multiple-Lapse Time Window Method. They showed that scattering (Q_s^{-1}) predominates over intrinsic Q^{-1} at low frequencies (1–4 Hz) for short hypocentral ranges (0–80 km) and intrinsic attenuation is dominant over scattering attenuation in all frequency bands for long hypocentral distances (80–170 km). Individual grabens in the region are composite basins and comprise multiple depocentres or subbasins with sediment thickness exceeding 3000 m in some locations and crossed by complicated fault systems (Çiftçi *et al.* 2010). This kind of structure near the surface could be responsible for the scattering attenuation in the region (Akıncı *et al.* 1995b). Low Q_o for large distances could indicate increasing density and velocities with depth. Increasing pressure

Downloaded from https://academic.oup.com/gji/article/195/2/1384/653885 by Dokuz Eylul University Library (DEU) user on 02 September 2021

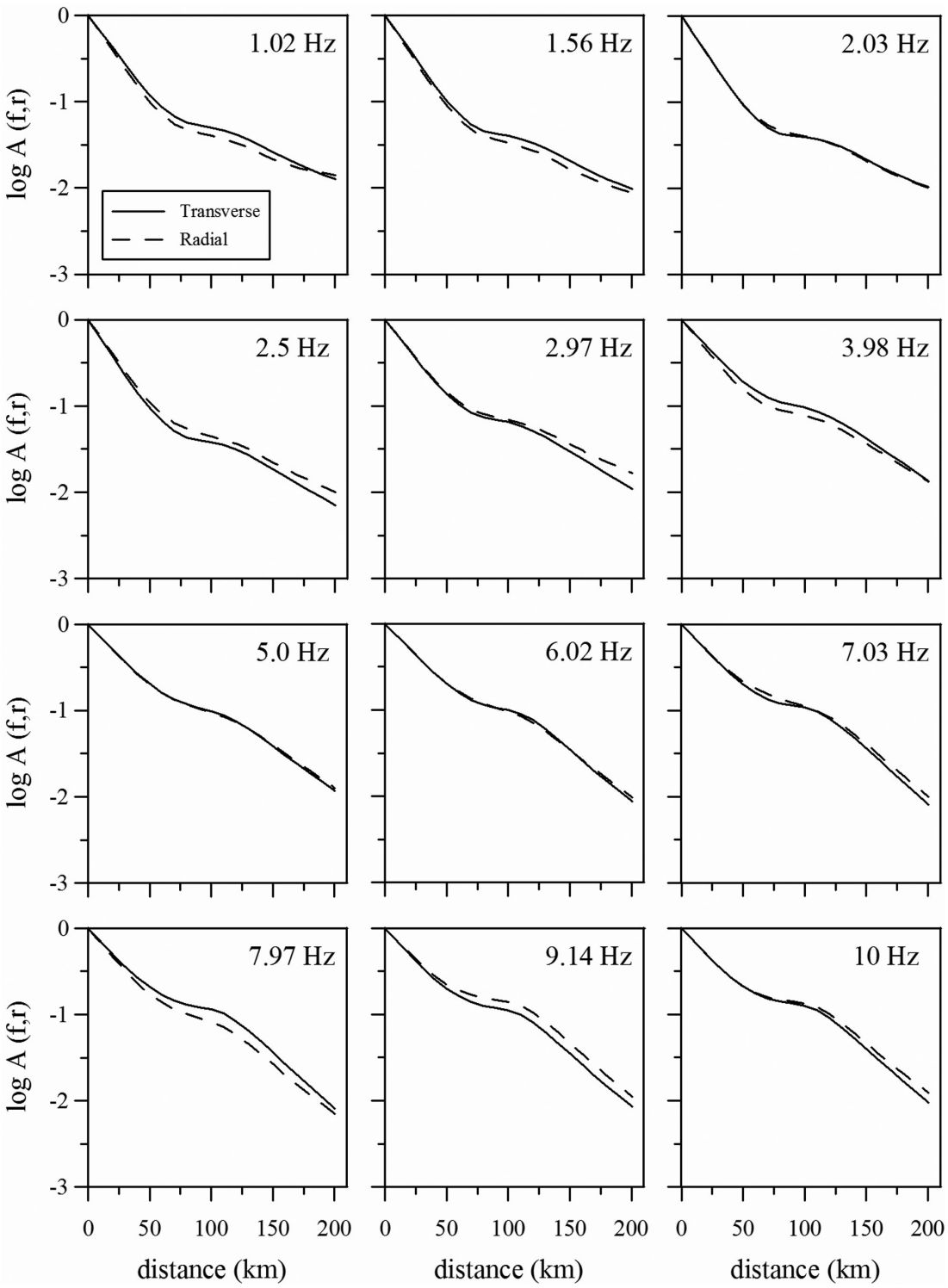


Figure 5. Comparison of the estimated non-parametric attenuation functions for 12 frequencies. Black and dashed lines represent *SH*- and *SV*-wave results, respectively.

and enhanced healing of cracks with increasing temperature and depth could explain these results (Mitchell & Xie 1994). The frequency dependencies of the transverse and radial S waves Q are $Q_{SH}(f) = 113.45(\pm 7.81) f^{0.47(\pm 0.04)}$ and $Q_{SV}(f) = 173.60(\pm 11.29) f^{0.28(\pm 0.04)}$ for greater distances. Different Q_o and n values may indicate Q anisotropy for deeper phases which could be associated to plastic flow at greater depth (Mitchell & Xie 1994).

Fig. 9 compares the b estimates for the transverse and radial S waves at two different distance ranges. At short distances b is approximately 0.9 ± 0.03 (Fig. 9a). Thus, for the 10–70 km range an average value of b seems adequate for the region within the frequency band of interest (1–10 Hz). Our estimates of b decrease significantly with increasing frequency in the 120–200 km distance range (Fig. 9b). Castro *et al.* (2009) has observed a similar

Downloaded from https://academic.oup.com/gji/article/195/2/1384/653885 by Dokuz Eylul University Library (DEU) user on 02 September 2021

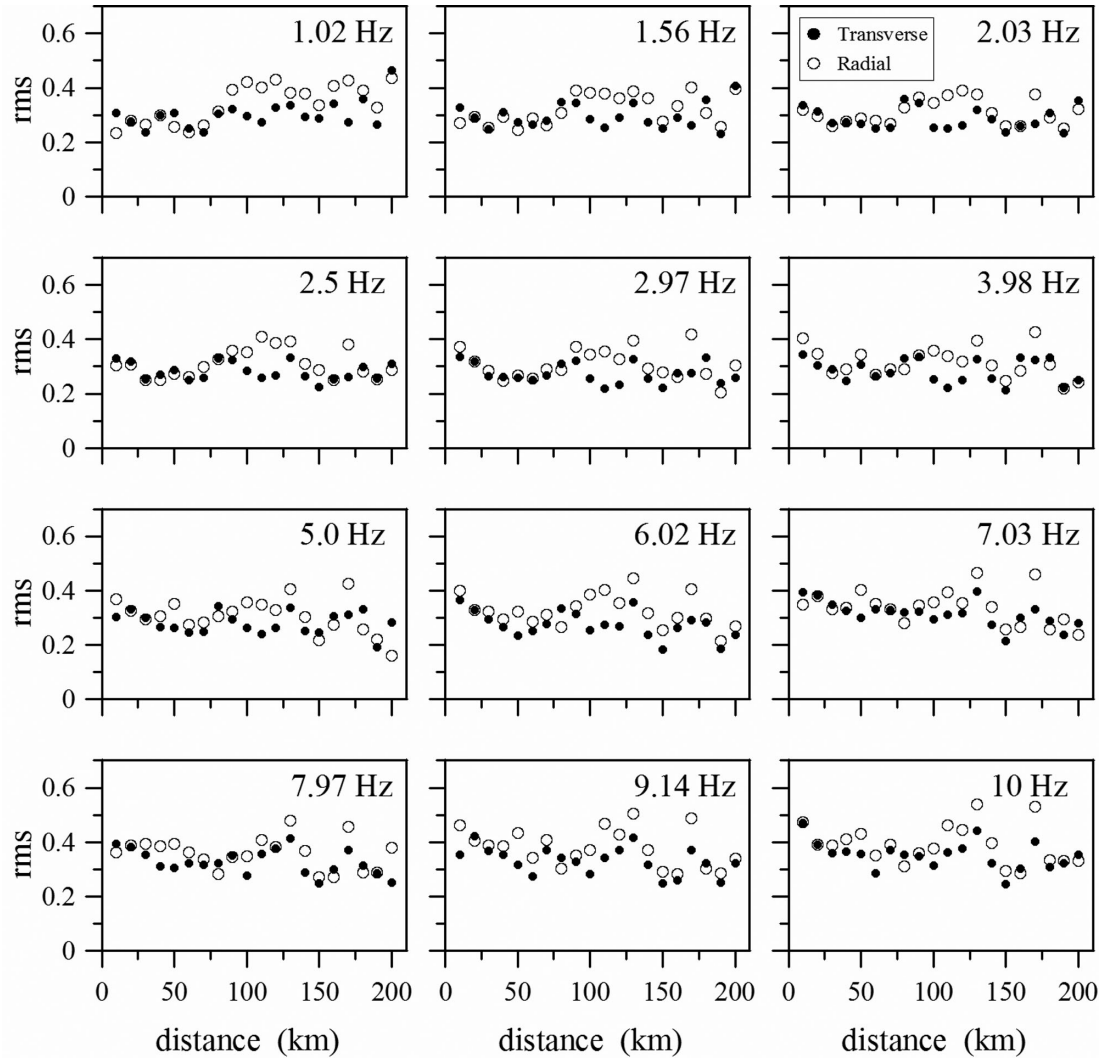


Figure 6. Note that *rms* values of residuals associated with the first inversion step in eq. (2) and the results in Fig. 5. Dots and circles represent *rms* values for *SH* and *SV* waves, respectively.

behaviour of the geometrical spreading exponent in the Sonora Basin and Range for the 40–80 km range, for both *P* and *S* waves. *F*-test statistics reveal that there are no statistically meaningful linear trends between exponent *b* values in whole frequency range of interest. Beyond 2 Hz, the exponent *b* decrease significantly from the value of 0.8 to 0.3. For that reason, we parametrize $b(f)$ values for two different frequency ranges: an average value of $b = 0.84(\pm 0.02)$ for $f \leq 2$ Hz; $b(f) = 1.43(\pm 0.11)\, f^{-072(\pm 0.06)}$ for $f > 2$ Hz for *SH* waves and an average value of $b = 0.93(\pm 0.06)$ for $f \leq 2$ Hz; $b(f) = 1.52(\pm 0.12)\, f^{-0.70(\pm 0.07)}$ for $f > 2$ Hz for *SV* waves. Decrease in *b* beyond 2 Hz for large distances could be explained by constructive interference of high-frequency refracted and reflected waves generated by geological complexity. In addition, the geometrical spreading probably starts having smaller effect on the amplitude decay because of surface wave arrivals at this long distance range.

Morozov (2010) showed that geometrical spreading is far from any of the theoretical 'spreading-wave front' models and contains pervasive 'multipathing' represented by multiple reflections and mode conversions because of the wavefields generated by complex crustal and mantle structure. Recent studies of body-wave attenuation where seismically active areas in the different parts of the world show that the value of the geometrical spreading coefficient associated with the distance may be more complicated than a simple assumption of $b = 1$, because of the complex velocity structure of the media. For instance, Castro *et al.* (2008b) modelled upper and lower crust total *Q* in the southern region of Italy. They investigated frequency dependence of geometrical spreading coefficient for lower crust. They obtained that the geometrical spreading varies between $r^{-0.3}$ and $r^{-0.5}$.

Obtained $Q(f)$ function for entire distance range was compared with the results for western Turkey and for different regions from all over the world in Figs 11(a) and (b), respectively. The average of our $Q_{SH}(f)$ and $Q_{SV}(f)$ estimates, $Q_S(f) = 190 \pm 13.5\, f^{0.64 \pm 0.05}$, is given in this figure. Using the single isotropic scattering model, Akıncı *et al.* (1994) obtained $Q_c(f) = 50.7 f^{1.01}$ for a lapse time of 30 s and $Q_c(f) = 183.2 f^{0.76}$ for a lapse time of 190 s for western Turkey. More than the central west Turkey, their data came from northwestern Turkey. Fig. 11(a) includes their Q_c estimates for a lapse time of 30 s. Based on the *S* wave to coda wave amplitude ratio with distance, Horasan & Boztepe-Güney (2004) computed Q_S values of the crust in the Sea of Marmara for a lapse time 50 s for five regions ranging from $13 \pm 1 f^{1.22 \pm 0.05}$ to $94 \pm 3 f^{0.83 \pm 0.04}$. An average of their estimates, $40 \pm 5\, f^{1.03 \pm 0.06}$ was

Downloaded from https://academic.oup.com/gji/article/195/2/1384/653885 by Dokuz Eylul University Library (DEU) user on 02 September 2021

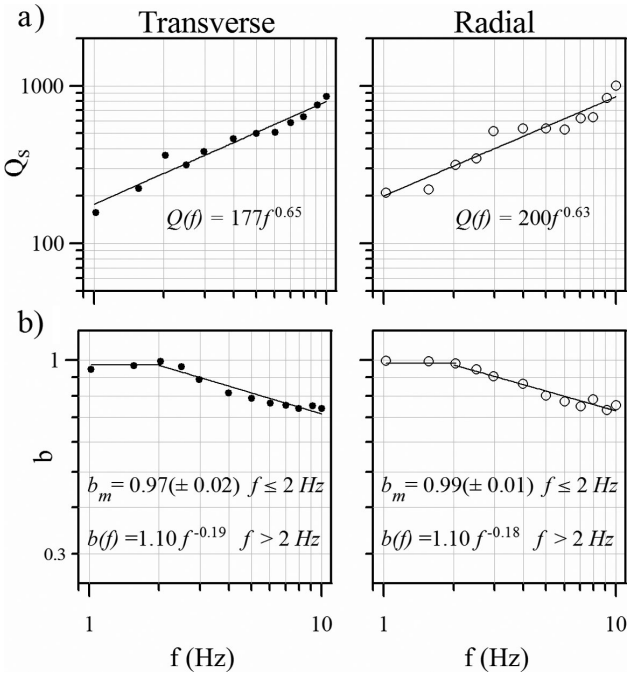


Figure 7. (a) Q and (b) b values versus frequency for the distance range between 10 and 200 km. Dots and circles represent Q and b values of *SH* and *SV* waves, respectively. b_m indicates the arithmetic mean of b values. $Q(f)$ and $b(f)$ present the least-square fits of the Q and b values.

given in Fig. 11(a). Akıncı *et al.* (2006) computed $Q_S(f) = 180 f^{0.45}$ (Fig. 11a) in the frequency range of 0.4–15.0 Hz and in the distance range of 10–200 km for the Marmara region, Turkey. They obtained a piecewise linear geometrical spreading function. Şahin

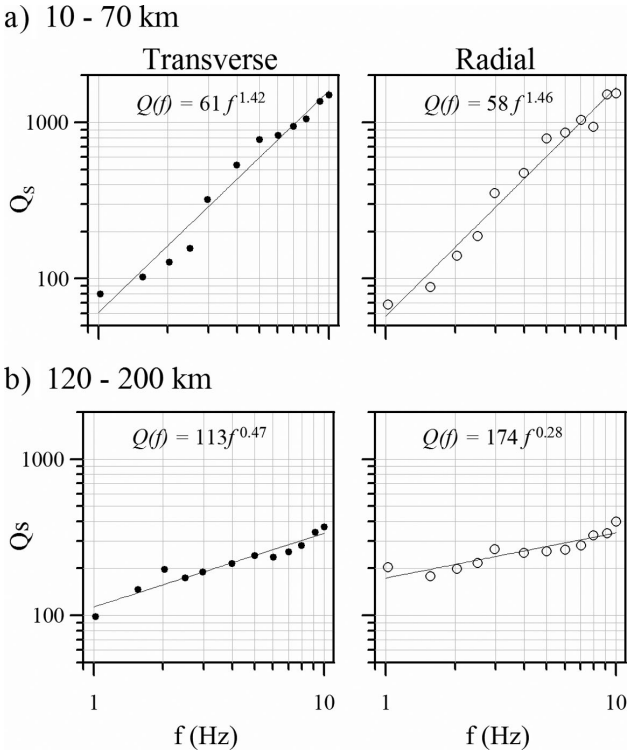


Figure 8. Q values for (a) short (10–70 km) and (b) long (120–200 km) distance ranges. Dots and circles represent Q values of *SH* and *SV* waves, respectively. Solid lines are the least-square fits of Q values.

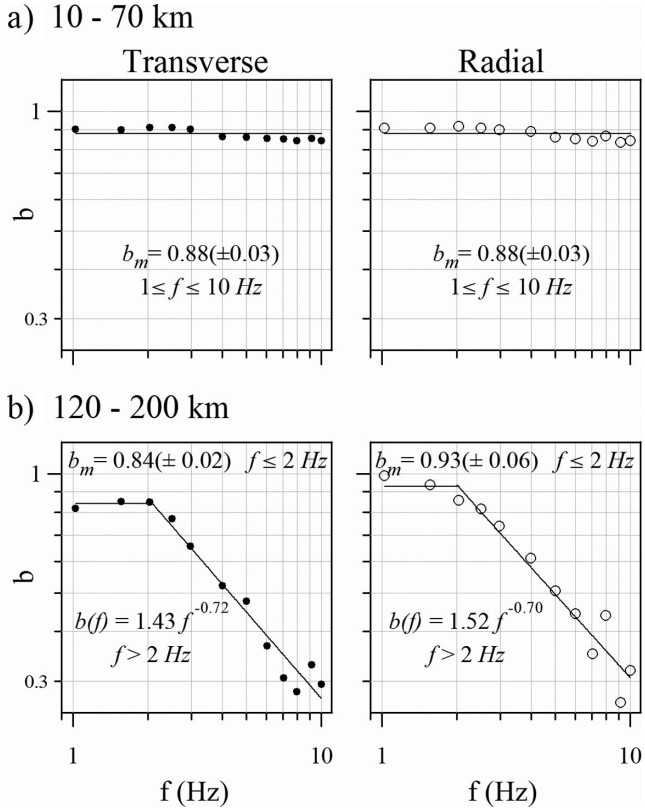


Figure 9. Note that b values for (a) short (10–70 km) and (b) long (120–200 km) distance ranges. Dots and circles represent b values of *SH* and *SV* waves, respectively. b_m indicates the arithmetic mean of b values. $b(f)$ presents the least-square fits of the b values.

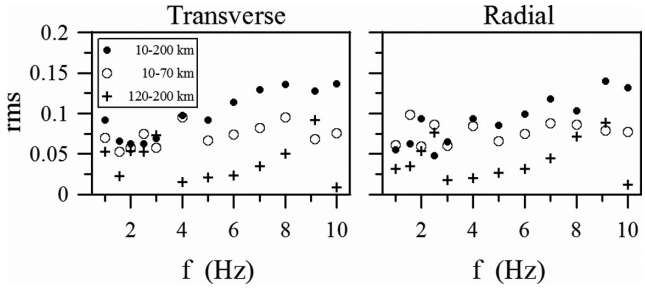


Figure 10. Note that *rms* values of residuals associated with the second inversion step in eq. (6) and the results in Figs 7, 8 and 9. Dots, circles, and crosses represent *rms* values for the distance ranges of 10–200 km, 10–70 km and 120–200 km, respectively.

et al. (2007) estimated intrinsic and scattering seismic attenuation in southwestern Anatolia by using coda-Q and the Multiple Lapse Time Window methods. Intrinsic; $Q_i(f) = 111 f^{1.17}$ and observed coda; $Q_C(f) = 125 f^{0.84}$ estimates from their results are given in Fig. 11(a). Akıncı *et al.* (2013) scaled ground motions in the frequency range of 0.25–10 Hz for western Turkey. Their data set contains our study area and data set as a subset. They obtained anelastic attenuation function $Q_S(f) = 180 f^{0.55}$ (Fig. 11a) with a piecewise geometrical spreading coefficient for the region.

Castro *et al.* (1999) obtained the frequency dependence of Q as $Q_{SV}(f) = 105.6 f^{0.65}$ and $Q_{SH}(f) = 86.1 f^{0.70}$ for the region of Marche, Italy. In Fig. 11(b), the average $Q_S(f)$ function of their $Q_{SV}(f)$ and $Q_{SH}(f)$ estimates was given. Malagnini *et al.* (2002)

Downloaded from https://academic.oup.com/gji/article/195/2/1384/653885 by Dokuz Eylul University Library (DEU) user on 02 September 2021

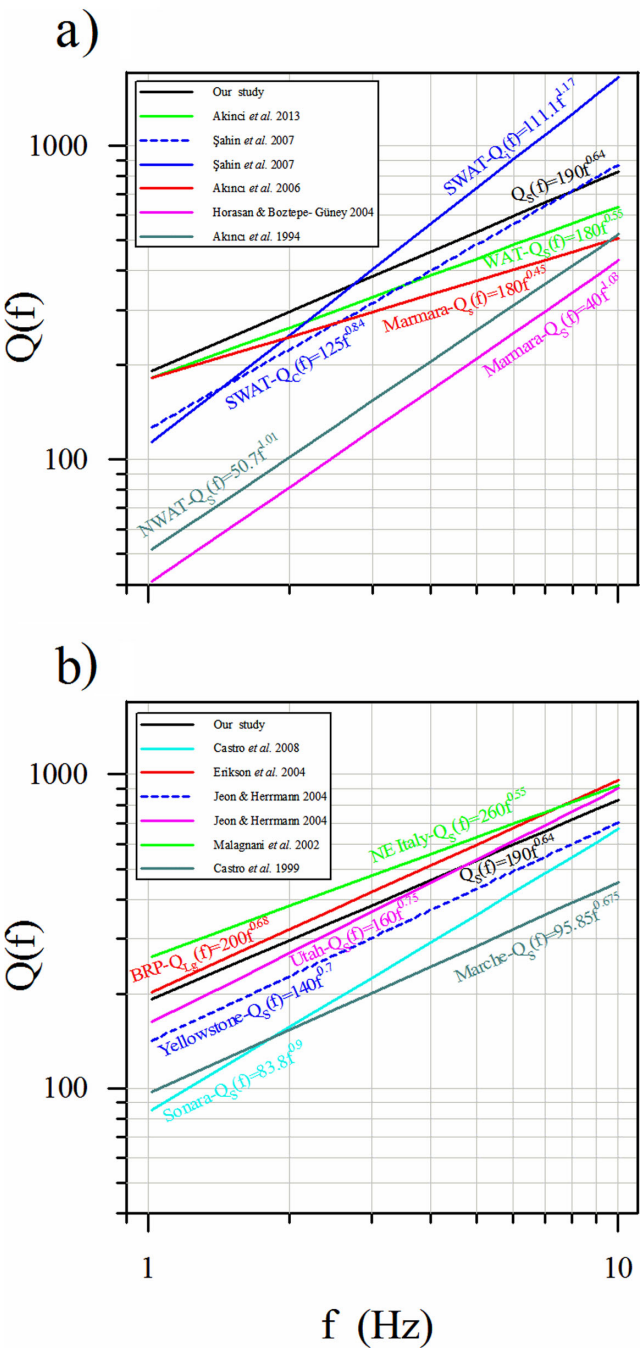


Figure 11. An average $Q(f)$ results (black line) for entire distance range (10–200 km) from this study compared to results from numerous regions (a) for vicinity of western Turkey: NWAT- $Q_S(f)$ (North Western Anatolia-Turkey; Akıncı *et al.* 1994), Marmara- $Q_S(f)$ (The Marmara Region-Turkey; Horasan & Boztepe-Güney 2004 and Akıncı *et al.* 2006), SWAT-$Q_i(f)$ and SWAT-$Q_C(f)$ (South Western Anatolia-Turkey; Şahin *et al.* 2007), WAT-$Q_S(f)$ (Western Anatolia-Turkey; Akıncı *et al.* 2013). (b) for different regions from all over the world: Marche-$Q_S(f)$ (Marche-Italy; Castro *et al.* 1999), NE Italy-$Q_S(f)$ (North East-Italy; Malagnini *et al.* 2002), BRP-$Q_{Lg}(f)$ (Basin and Range Province-USA; Erickson *et al.* 2004), Utah and Yellowstone-$Q_S(f)$ (USA; Jeon & Herrmann 2004), Sonora-$Q_S(f)$ (Northeastern Sonora-Mexico; Castro *et al.* 2008c).

computed $Q_S(f) = 260\, f^{0.55}$ (Fig. 11b) in the frequency range of 0.5–14.0 Hz together with a slightly frequency-dependent geometrical spreading for northeastern Italy. Jeon & Herrmann (2004) estimated the anelastic attenuation functions $Q_S(f) = 160\, f^{0.75}$ and $Q_S(f) = 140\, f^{0.70}$ with a piecewise geometrical spreading coefficient for Utah (Basin and Range Province) and for the Yellowstone region, respectively. Their $Q_S(f)$ estimates are given in Fig. 11(b). Erickson *et al.* (2004) compared L_g attenuation between seven different tectonic regions in the continental United States. They obtained $Q_{Lg}(f) = 200(\pm 40)\, f^{0.68(\pm 0.12)}$ (Fig. 11b) for the Basin and Range Province in the frequency band 0.5–16 Hz. Castro *et al.* (2008c) computed $Qs(f) = 83.8\, f^{0.9}$ (Fig. 11b) in the frequency range of 0.4–63.1 Hz in Northeastern Sonora, Mexico. In the region of Sonoran Basin and Range, they obtained that *P* waves attenuate more than *S* waves.

As shown in Fig. 11(a), Akıncı *et al.* (2013) obtained quite similar Q values ($Q_S(f) = 180\, f^{0.55}$) with our result ($Q_S(f) = 190 \pm 13.5 f^{0.64 \pm 0.05}$). The slight differences between the results could be caused different parametrizations, employed data sets and the methodologies used (Ford *et al.* 2008). For instance, their data set includes our study area as a subregion and consists of recordings from 902 regional earthquakes of magnitude 2.5–5.8 and the distance range of 15–250 km. They used narrow bandpass-filtered time histories around the fixed frequencies and computed a duration window for each filtered time history. They obtained a piecewise geometrical spreading coefficient (1.0 for $1 < r < 20$ km; 0.8 for $20 < r < 40$ km; 0.7 for $40 < r < 100$ km and 0.5 for $r > 100$ km) for the region. Both of the anelastic attenuation functions for the Basin and Range Province from Erickson *et al.* (2004) and Jeon & Herrmann (2004) are quite similar with ours (Fig. 11b). In recent years, the Aegean extensional region has been compared to Basin & Range province (e.g. Zhu *et al.* 2006a) because both of them were evaluated as the metamorphic core complexes. Large scale extension, high heat flow and thin continental crust in a tectonically active subduction system environment have characterized both of the regions.

5 CONCLUSIONS

This paper presents crustal attenuation characteristics in the central part of west Turkey by using a two-step inversion. In the first step, we obtained non-parametric attenuation functions for *SH* and *SV* waves. In the second step, we analysed the behaviour of anelastic attenuation Q and the geometrical spreading exponent b at different frequencies for three different distance range. The b values for the transverse and radial *S* waves are 0.9 ± 0.03 for short paths (10–70 km) within the frequency band of interest. We modelled b frequency dependence as a piecewise in two frequency ranges for entire (10–200 km) and long (120–200 km) distance ranges. These results one more time emphasizes that geometrical spreading can only be associated with the time or distance dependence of the wavefield rather than any particular seismic phase.

We explored spatial variations of Q to infer anisotropy and analysed possible causes. Note that, we obtained average values for the attenuation functions in the region without any azimuthal information contained in each recording. Low Q_0 values and strong frequency dependence of Q at short hypocentral distances (10–70 km) could be associated to strong heterogeneity because of high degree of fracturing, fluid filled cracks, young volcanism and/or geothermal activity in the crust. Lower Q frequency dependence and higher Q_0 values manifest more homogenous medium because of increasing

Downloaded from https://academic.oup.com/gji/article/195/2/1384/653885 by Dokuz Eylul University Library (DEU) user on 02 September 2021

density and pressure along with depth for large hypocentral ranges (120–200 km). Q values obtained for *SH* and *SV* waves do not show significant differences for the distance range between 10 and 70 km. However, in the distance range between 120 and 200 km, $Q_{SV}(f)$ has higher Q_0 value and lower frequency dependence than $Q_{SH}(f)$. This Q anisotropy could be associated to plastic flow at greater depth contributing to the dissipation of cracks in the extensional intracontinental plate setting of the region.

ACKNOWLEDGEMENTS

This paper is a part of a Ph.D. thesis undertaken by Tevfik Özgür Kurtulmuş at the Institute of Natural and Applied Sciences in Dokuz Eylül University (DEU). It is supported by DEU Scientific Research Foundation Grant BAP-Project No: 2008.KB.FEN.08. Fig. 2 was produced using public domain software 'Generic Mapping Tools' (GMT; Wessel & Smith 1995). We thank WASRE network team for their dedicated efforts during data collection stage. We also thank Brian J. Mitchell, Raul R. Castro, Talip Güngör, Lupei Zhu, Aybige Akıncı and Sebastiano D'Amico for their contributions. We are grateful to Raul R. Castro and an anonymous reviewer whose comments and suggestions have significantly improved the manuscript.

REFERENCES

Akıncı, A., Taktak, G. & Ergintav, S., 1994. Attenuation of coda waves in the western Anatolia, *Phys. Earth planet. Inter.,* **87,** 155–165.

Akıncı, A., Ibanez, J.M., Del Pezzo, E. & Morales, J., 1995a. Geometrical spreading and attenuation of Lg waves: a comparison between western Anatolia (Turkey) and southern Spain, *Tectonophysics,* **250,** 47–60.

Akıncı, A., Del Pezzo, E. & Ibanez, J.M., 1995b. Separation of scattering and intrinsic attenuation in southern Spain and western Anatolia (Turkey), *Geophys. J. Int.,* **121,** 337–353.

Akıncı, A. & Eyidoğan, H., 1996. Frequency-dependent attenuation of S and coda waves in Erzincan region (Turkey), *Phys. Earth planet. Inter.,* **97,** 109–119.

Akıncı, A., Mejia, J. & Jemberie, A., 2004. Attenuative disperision of P waves and crustal Q in Turkey and Germany, *Pure appl. Geophys.,* **161,** 73–91.

Akıncı, A., D'Amico, S., Malagnini, L. & Mercuri, A., 2013. Scaling earthquake ground motions in the western Anatolia, Turkey, *Phys. Chem. Earth,* in press, doi:10.1016/j.pce.2013.04.013.

Akıncı, A., Malagnini, L., Herrmann, R.B., Gok, R. & Sørensen, M.B., 2006. Ground motion scaling in the Marmara region, Turkey, *Geophys. J. Int.,* **166,** 635–651.

Akyol, N., Akıncı, A. & Eyidoğan, H., 2002. Separation of source, propagation and site effects from S waves of local earthquakes in Bursa region, northwestern Turkey, *Pure appl. Geophys.,* **159,** 1253–1269.

Akyol, N., Kurtulmuş, T.Ö., Çamyıldız, M. & Güngör, T., 2013. Spectral ratio estimates for site effects on the horst–graben system in west Turkey, *Pure appl. Geophys.,* in press, doi:10.1007/s00024-013-0661-2.

Akyol, N., Zhu, L., Mitchell, B.J., Sözbilir, H. & Kekovalı, K., 2006. Crustal structure and local seismicity in western Anatolia, *Geophys. J. Int.,* **166**(3), 1259–1269.

Aldanmaz, E., 2002. Mantle source characteristics of alkali basalts and basanites in an extensional intracontinental plate setting, western Anatolia, Turkey: implications for multi-stage melting, *Int. Geol. Review,* **44**(5), 440–457.

Aldanmaz, E., 2006. Mineral-chemical constraints on the Miocene calc-alkaline and shoshonitic volcanic rocks of western Turkey: disequilibrium phenocryst assemblages as indicators of magma storage and mixing conditions, *Turkish J. Earth Sci.,* **15,** 47–73.

Atkinson, G. & Mereu, R., 1992. The shape of ground motion attenuation curves in southeastern Canada, *Bull. seism. Soc. Am.,* **82,** 2014–2031.

Bindi, D., Parolai, S., Grosser, S., Milkereit, C. & Karakısa, S., 2006. Crustal attenuation characteristics in northwestern Turkey in the range from 1 to 10 Hz, *Bull. seism. Soc. Am.,* **96**(1), 200–214.

Boztepe-Güney, A. & Horasan, G., 2002. Enhanced ground motions due to large-amplitude critical Moho reflections (SmS) in the Sea of Marmara, Turkey, *Geophys. Res. Lett.,* **29,** 9-1–9-4.

Castro, R.R., Anderson, J.G. & Singh, S.K., 1990. Site response, attenuation and source spectra of S waves along the Guerrero, Mexico, subduction zone, *Bull. seism. Soc. Am.,* **80**(6), 1481–1503.

Castro, R.R., Gallipoli, M.R. & Mucciarelli, M., 2008b. Crustal Q in southern Italy determined from regional earthquakes, *Tectonopyhsics,* **457,** 96–101.

Castro, R.R., Massa, M., Augliera, P. & Pacor, F., 2008a. Body-wave attenuation in the region of Garda, Italy, *Pure appl. Geophys.,* **165,** 1351–1366.

Castro, R.R., Condori, C., Romero, O., Jacques, C. & Suter, M., 2008c. Seismic attenuation in northeastern Sonora, Mexico, *Bull. seism. Soc. Am.,* **98**(2), 722–732.

Castro, R.R., Monachesi, G., Mucciarelli, M., Trojani, L. & Pacor, F., 1999. P- and S-wave attenuation in the region of Marche, Italy, *Tectonophysics,* **302,** 123–132.

Castro, R.R., Huerta, C.I., Romero, O., Jacques, C., Hurtado, A. & Fernández, A.I., 2009. Body-wave attenuation near the rupture of the 1887 Sonora, México, earthquake (Mw 7.5), *Geofisica Internacional,* **48**(3), 297–304.

Çiftçi, N.B., Temel, R.O. & İztan, Y.H., 2010. Hydrocarbon occurrences in the western Anatolian (Aegean) grabens, Turkey: is there a working petroleum system? *AAPG Bull.,* **94**(12), 1827–1857.

Cong, L. & Mitchell, B.J., 1998. Lg Coda Q and its relation to the geology and tectonics of the Middle East, *Pure appl. Geophys.,* **153,** 563–585.

Erickson, D., McNamara, D.E. & Benz, H.M., 2004. Frequency dependent Lg Q within the continental United States, *Bull. seism. Soc. Am.,* **94**(5), 1630–1643.

Ford, S.R., Dreger, D.S., Mayeda, K., Walter, W.R., Malagnini, L. & Phillips, W.R., 2008. Regional attenuation in northern California: a comparison of five 1D Q methods, *Bull. seism. Soc. Am.,* **98**(4), 2033–2046.

Gessner, K., Ring, U., Johnson, C., Hetzel, R., Passchier, C.W. & Güngör, T., 2001. An active bivergent rollinhinge detachment system. Central Menderes metamorphic core complex in western Turkey, *Geology,* **29,** 611–614.

Gürer, A. & Bayrak, M., 2007. Relation between electrical resistivity and earthquake generation in the crust of west Anatolia, Turkey, *Tectonophysics,* **445,** 49–65.

Horasan, G. & Boztepe-Güney, A., 2004. S-wave attenuation in the Sea of Marmara, Turkey, *Phys. Earth planet. Inter.,* **142,** 215–224.

Horasan, G., Kaşlılar-Özcan, A., Boztepe-Güney, A. & Niyazi, T., 1998. S-wave attenuation in the Marmara Sea, northwestern Turkey, *Geophys. Res. Lett.,* **25,** 2733–2736.

Ibáñez, J.M., Del Pezzo, E., Alguacil, G., De Miguel, F., Morales, J., De Martino, S., Sabbarese, C. & Posadas, A.M., 1993. Geometrical spreading function for short-period S and coda waves recorded in southern Spain, *Phys. Earth planet. Inter.,* **80,** 25–36.

Jeon, Y.S. & Herrmann, R.B., 2004. High-frequency earthquake ground-motion scaling in Utah and Yellowstone, *Bull. seism. Soc. Am.,* **94**(5), 1644–1657.

Kaşlılar-Özcan, A., Boztepe-Güney, A. & Ecevitoğlu, B., 2002. Estimation of attenuation structure in the Çınarcık Basin of the Marmara Sea, northwest Turkey, *Phys. Earth planet. Inter.,* **130,** 1–16.

Malagnini, L., Akıncı, A., Herrmann, R.B., Pino, N.A. & Scognamiglio, L., 2002. Characteristics of the ground motion in northeastern Italy, *Bull. seism. Soc. Am.,* **92**(6), 2186–2204.

Menke, W., 1989. *Geophysical Data Analysis: Discrete Inverse Theory,* Vol. 45, pp. 289, Academic Press.

Mitchell, B.J. & Xie, J., 1994. Attenuation of multiphase surface waves in the basin and range province-III. Inversion for crustal anelasticity, *Geophys. J. Int.,* **116**(2), 468–484.

Downloaded from https://academic.oup.com/gji/article/195/2/1384/653885 by Dokuz Eylul University Library (DEU) user on 02 September 2021

Morozov, I.B., 2010. *Seismological Attenuation Without Q,* pp. 376, Trafford Publishing.

Mutlu, H., 2007. Constraints on the origin of the Balıkesir thermal waters (Turkey) from stable isotope (δ^{18}O, δD, δ^{13}C, δ^{34}S) and major-trace element compositions, *Turkish J. Earth Sci.,* **16,** 13–32.

Olafsson, S., Sigbjörnsson, R. & Einarsson, P., 1998. Estimation of source parameters and Q from acceleration recorded in the Vatnafjöll earthquake in south Iceland, *Bull. seism. Soc. Am.,* **88,** 556–563.

Oral, M.B., Reilinger, R.E., Toksöz, M.N., King, R.W., Barka, A.A., Kınık, İ. & Lenk, O., 1995. Global positioning system offers evidence of plate motions in eastern Mediterranean, *EOS Trans.,* **76**(2), 9–11.

Padhy, S., 2009. Characteristics of body-wave attenuations in the Bhuj Crust, *Bull. seism. Soc. Am.,* **99**(6), 3303–3313.

Rojay, B., Toprak, V., Demirci, C. & Süzen, L., 2005. Plio-Quaternary evolution of the Küçük Menderes graben southwestern Anatolia, Turkey, *Geodinamica Acta,* **18**(3–4), 317–331.

Şahin, Ş., Erduran, M., Alptekin, Ö. & Çakır, Ö., 2007. Intrinsic and scattering seismic attenuation in southwestern Anatolia, *Pure appl. Geophys.,* **164,** 2255–2270.

Şahin, Ş., 2008. Lateral variations of coda Q and attenuation of seismic waves in southwest Anatolia, *J. Seismol.,* **12,** 367–376.

Şahin, Ş., Bao, X., Türkelli, N., Sandvol, E., Teoman, U. & Kahraman, M., 2013. Lg wave attenuation in the Isparta angle and Anatolian plateau (Turkey), *Pure appl. Geophys.,* **170,** 337–351.

Saunders, P., Priestly, K. & Taymaz, T., 1998. Variations in the crustal structures beneath western Turkey, *Geophys. J. Int.,* **134,** 373–389.

Şengör, A.M.C., Satır, M. & Akkök, R., 1984. Timing of the tectonic events in the Menderes massif, western Turkey: implications for tectonic evolution and evidence for Pan-African basement in Turkey, *Tectonics,* **3,** 693–707.

Sereno, T.J. & Given, J.W., 1990. P_n attenuation for a spherically symmetric Earth model, *Geophys. Res. Lett.,* **17,** 1141–1144.

Seyitoğlu, G. & Işık, V., 2009. Meaning of the Küçük Menderes graben in the tectonic framework of the central Menderes metamorphic core complex (western Turkey), *Geologica Acta,* **7**(3), 323–331.

Sonley, E. & Atkinson, G.M., 2006. Path-specific attenuation in eastern Canada, *Bull. seism. Soc. Am.,* **96**(4A), 1375–1382.

Tarcan, G., Filiz, S. & Gemici, U., 2000. Geology and geochemistry of the Salihli geothermal fields, Turkey, in *Proceedings of World Geothermal Congress,* Kyushu-Tohoku, Japan, 28 May–June 10, 2000, pp. 1829–1834, Abstracts Book.

Tokçaer, M., Agostini, S. & Savasçın, M.Y., 2005. Geotectonic setting and origin of the youngest Kula volcanics (western Anatolia), with a new emplacement model, *Turkish J. Earth Sci.,* **14,** 145–166.

Uzel, B., Sözbilir, H. & Özkaymak, Ç., 2012. Neotectonic evolution of an actively growing superimposed basin in western Anatolia: the inner bay of İzmir, Turkey, *Turkish J. Earth Sci.,* **21,** 439–471.

Wessel, P. & Smith, W.H.F., 1995. New version of the generic mapping tools released, *EOS Trans. AGU,* **76**(33), 329.

Yang, X., Lay, T., Xie, X.B. & Thorne, M.S., 2007. Geometric spreading of *Pn* and *Sn* in a spherical Earth model, *Bull. seism. Soc. Am.,* **97,** 2053–2065.

Yılmaz, Y., Genç, S.C., Gürer, O.F., Bozcu, M., Yılmaz, K., Karacık, Z., Aktunkaynak, Ş. & Elmas, A., 2000. When did the western Anatolian grabens begin to develop? in *Tectonics and Magmatism in Turkey and the Surrounding Area,* pp. 353–384, eds Bozkurt, E., Winchester, J.A. & Piper, J.D.A., Geol. Soc. London Spec. Pub.

Zhu, L., Mitchell, B.J., Akyol, N., Çemen, I. & Kekovalı, K., 2006a. Crustal thickness variation in the Aegean region and its implications for the extension of continental crust, *J. geophys. Res.,* **111,** B01301, doi:10.1029/2005JB003770.

Zhu, L., Akyol, N., Mitchell, B.J. & Sözbilir, H., 2006b. Seismotectonics of western Turkey from high resolution earthquake relocations and moment tensor determinations, *Geophys. Res. Lett.,* **33,** L07316, doi:10.1029/2006GL025842.

Zor, E., Sandvol, E., Gurbuz, C., Turkelli, N., Seber, D. & Barazangi, M., 2003. The crustal structure of the east Anatolian plateau from receiver functions, *Geophys. Res. Lett.,* **30,** 8044, doi:10.1029/2003GL018192.

Zor, E., Sandvol, E., Xie, J.K., Türkeli, N., Mitchell, B.J., Gasanov, A.H. & Yetirmishli, G., 2007. Crustal attenuation within the Turkish plateau and surrounding regions, *Bull. seism. Soc. Am.,* **97**(1B), 151–161.

Downloaded from https://academic.oup.com/gji/article/195/2/1384/653885 by Dokuz Eylul University Library (DEU) user on 02 September 2021